

RESEARCH ARTICLE | DECEMBER 18 2023

## Integrated control of edge localized modes and divertor flux using mixed toroidal harmonic resonant magnetic perturbations in EAST

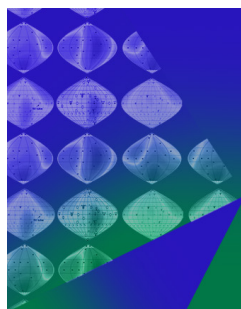
Qun Ma ; You-Wen Sun ; Man-Ni Jia ; Shuai Gu ; Xue-Min Wu ; Peng-Cheng Xie ; Carlos Paz-Soldan ; Yun-Feng Liang ; Fang-Chuan Zhong ; Liang Wang ; Fang Ding ; Bin Zhang ; Tong-Hui Shi ; Biao Shen ; Hui-Hui Wang ; Ling Zhang ; Yu-Min Wang ; Qing Zang ; Ying-Ying Li ; Yue-Qiang Liu ; Bao-Nian Wan 



*Phys. Plasmas* 30, 122507 (2023)

<https://doi.org/10.1063/5.0170003>





## Physics of Plasmas

### Features in Plasma Physics Webinars

Register Today!



# Integrated control of edge localized modes and divertor flux using mixed toroidal harmonic resonant magnetic perturbations in EAST

Cite as: Phys. Plasmas **30**, 122507 (2023); doi: 10.1063/5.0170003

Submitted: 31 July 2023 · Accepted: 29 November 2023 ·

Published Online: 18 December 2023



View Online



Export Citation



CrossMark

Qun Ma,<sup>1,2</sup> You-Wen Sun,<sup>1,a)</sup> Man-Ni Jia,<sup>1,a)</sup> Shuai Gu,<sup>3</sup> Xue-Min Wu,<sup>1,2</sup> Peng-Cheng Xie,<sup>1,2</sup> Carlos Paz-Soldan,<sup>4</sup> Yun-Feng Liang,<sup>5</sup> Fang-Chuan Zhong,<sup>6</sup> Liang Wang,<sup>6</sup> Fang Ding,<sup>1</sup> Bin Zhang,<sup>1</sup> Tong-Hui Shi,<sup>1</sup> Biao Shen,<sup>1</sup> Hui-Hui Wang,<sup>1</sup> Ling Zhang,<sup>1</sup> Yu-Min Wang,<sup>1</sup> Qing Zang,<sup>1</sup> Ying-Ying Li,<sup>7,8</sup> Yue-Qiang Liu,<sup>9</sup> and Bao-Nian Wan<sup>1</sup>

## AFFILIATIONS

<sup>1</sup>Institute of Plasma Physics, Hefei Institutes of Physical Science, Chinese Academy of Sciences, Hefei 230031, China

<sup>2</sup>Science Island Branch, Graduate School of University of Science and Technology of China, Hefei 230026, China

<sup>3</sup>Oak Ridge Associated Universities, Oak Ridge, Tennessee 37831, USA

<sup>4</sup>Department of Applied Physics and Applied Mathematics, Columbia University, New York, New York 10027, USA

<sup>5</sup>Institut für Energie- und Klimaforschung - Plasmaphysik, Partner of the Trilateral Euregio Cluster (TEC), Forschungszentrum Jülich GmbH, Jülich 52425, Germany

<sup>6</sup>College of Science, Donghua University, Shanghai 201620, China

<sup>7</sup>Enn Science and Technology Development Co., Ltd, Langfang 065001, China

<sup>8</sup>Hebei Key Laboratory of Compact Fusion, Langfang 065001, China

<sup>9</sup>General Atomics, P.O. Box 85608, San Diego, California 921865608, USA

<sup>a)</sup>Authors to whom correspondence should be addressed: ywsun@ipp.ac.cn and jiamanni@ipp.ac.cn

## ABSTRACT

Mixed harmonic resonant magnetic perturbations (RMPs) for integrated edge localized modes (ELMs) and divertor flux control are demonstrated in EAST target plasmas of low input torque and normalized beta  $\beta_N \sim 1.7$ – $1.9$ , which are close to the equivalent value in ITER high Q operation. The applied RMPs are designed to combine a static harmonic of the toroidal mode number  $n = 3$  with a static or rotating harmonic of  $n = 2$ . ELM suppression is achieved without a drop of plasma energy confinement, and tungsten concentration is effectively reduced during the application of RMPs. With mixed harmonics, the toroidal varying steady state heat and particle fluxes on the divertor target can be modified with the rotating  $n = 2$  harmonic, which agrees with the numerical modeling of three-dimensional magnetic topology, with plasma responses being taken into account. ELM suppression correlates with the times of larger  $n = 3$  response with mixed  $n = 2$  and  $n = 3$  RMPs. The mixture of harmonics and the rotating  $n = 2$  harmonic does not require additional coil current because the variation is only in the upper-lower coil current phase space. These results further affirm the effectiveness of integrated ELM and divertor flux control using RMPs with mixed harmonics and improve the understanding of the role of plasma responses in ELM suppression.

Published under an exclusive license by AIP Publishing. <https://doi.org/10.1063/5.0170003>

## I. INTRODUCTION

The finding of high confinement (H-mode) plasmas<sup>1</sup> makes tokamak a promising device for controlled fusion power. The enhanced confinement is mainly due to the formation of the edge transport barrier that has a steep pressure gradient at the pedestal region. However, the free energy in the pedestal region may excite one kind of magnetohydrodynamic (MHD) instabilities known as edge localized modes (ELMs).<sup>2</sup> ELMs cause repetitive crashes of the pedestal and release a significant

fraction of thermal energy and particles in a few hundred microseconds to plasma facing components (PFCs) of a device, especially divertor targets. ELMy H-mode is chosen as the baseline scenario for the future fusion device ITER,<sup>3</sup> and the energy fluence on the divertor induced by each type-I ELM (the most serious one) is predicted<sup>4–6</sup> to be about  $10 \text{ MJ/m}^2$ , which far exceeds the allowed maximal limit ( $0.15 \text{ MJ/m}^2$ ) for current materials and will reduce lifetime of the PFCs.<sup>7,8</sup> Control of transient heat and particle fluxes induced by type-I ELMs is an essential issue in ITER.

Resonant magnetic perturbations (RMPs) produced by coils outside the plasma have been demonstrated as a promising technique for type-I ELM control in many tokamaks. DIII-D,<sup>9,10</sup> KSTAR,<sup>11</sup> EAST,<sup>12</sup> and ASDEX-Upgrade<sup>13</sup> have achieved fully ELM suppression, while ELM mitigation (the control of ELMs achieving a state of higher frequency and lower amplitude compared with natural ELMs) was achieved in all above-mentioned tokamaks as well as in JET,<sup>14</sup> MAST,<sup>15</sup> etc. Due to the uncertainty of the sufficiency of ELM mitigation for the transient power load reduction requirement in ITER, ELM suppression is focused. Most of these experiments use RMP fields with a single toroidal mode number  $n$ . Compared to those with high mode numbers, with the same field strength, RMPs with low  $n$  (e.g.,  $n = 1$  or  $2$ ) generate stronger resonant harmonics, which are favored for achieving ELM suppression but have larger impact on the core MHD stability and the confinement.<sup>16,17</sup> With regard to the requirement of energy and particle confinement for ITER high  $Q$  operation, RMPs with higher mode number,  $n = 3$  or  $4$ , are considered for ITER ELM suppression.<sup>18</sup> Although the ELM induced transient heat load can be suppressed by RMPs, the toroidal asymmetric spiral magnetic footprint due to lobe structures<sup>19</sup> induced by RMPs near the X point may introduce toroidal varying particle and heat fluxes with multiple stripes on the divertor target.<sup>20</sup> To avoid heat accumulation on a fixed area, it is necessary to spread the heat and particle fluxes on the divertor target during the RMP application while maintaining ELM suppression.<sup>18</sup> Rotating or spectrum adjusting of RMP has been demonstrated recently as a promising method<sup>21–24</sup> in spreading or modifying the steady state particle and heat flux on the divertor. However, this method requires oscillation of the full magnitude of the RMP current, which may threaten the lifetime of coils due to cyclic mechanical stress.

Joint experiments on both DIII-D and EAST have shown the potential of using mixed harmonic RMPs in ELM and divertor power load control,<sup>25,26</sup> which were motivated by the ELM suppression in DIII-D using a reduced number of I-coils.<sup>27</sup> Previous studies on DIII-D demonstrated that the mixed  $n = 2$  and  $3$  RMPs reduced the threshold coil current for ELM suppression<sup>28</sup> and the rotating  $n = 2$  harmonic spread the heat and particle fluxes on divertor target while maintaining ELM suppression.<sup>25</sup> With this method, only the  $n = 2$  harmonic is rotated. Therefore, it requires less change of coil current than that in the single  $n$  rotating RMP case and the sign of the current does not change, which makes the stress on the bracket from the interaction between RMP and equilibrium magnetic field to be always in the same direction, thus easing engineering limits on the coil lifetime.

In this paper, the demonstration of using a mixed harmonic RMPs for the integrated control of ELMs and steady state divertor heat and particle fluxes in EAST low input torque plasmas is presented. Static  $n = 3$  and static or rotating  $n = 2$  harmonics are combined. This is an extension of the mixed harmonics scheme used in EAST and DIII-D to low torque input plasmas close to ITER  $Q = 10$  scenarios. The input neutral beam injection (NBI) torque in EAST,  $T_{NBI,E}$  (about 1.1 Nm), is equivalent to the NBI torque in ITER high fusion gain  $Q = 10$  scenarios as the calculation in Ref. 16. In these experiments, the  $\beta_N \sim 1.7$ – $1.9$  are close to ITER  $Q = 10$  scenarios with  $\beta_N$  of about 1.8<sup>29</sup> and the safety factor at a 95% poloidal flux  $q_{95} \sim 3.7$  are close to the low  $q_{95} \sim 3$  requirements in such scenarios. The target plasmas are also similar to the full suppression of type-I ELMs using  $n = 4$  RMPs in the EAST experiment.<sup>16</sup> In DIII-D, it is still hard to achieve ELM suppression in low torque plasmas.<sup>30,31</sup>

The rest of this paper is organized as follows: The introduction of RMP system, experimental setup, and modeling approach are presented in Sec. II. ELM suppression with mixed  $n = 2$  and  $3$  RMPs compared with that using single  $n = 2$  or  $n = 3$  RMPs is presented in Sec. III. Dynamical divertor flux modification with rotating  $n = 2$  component together with ELM suppression maintained by mixed  $n = 2$  and  $3$  RMPs is given in Sec. IV, followed by a summary and conclusion in Sec. V.

## II. EXPERIMENTAL SETUP AND MODELING APPROACH

EAST is a fully superconducting tokamak with a major radius  $R \approx 1.85$  m and a minor radius  $a \approx 0.45$  m, aiming for long pulse operation.<sup>32</sup> Radio-frequency (RF) wave dominant heating makes EAST a unique tokamak to access ELM suppression with low input torque.<sup>12,33</sup> ELM suppression in low input torque plasmas was then achieved in a low torque scenario with co- & ctr-NBI and lower hybrid wave (LHW) obtained in EAST.<sup>16</sup>

### A. Experimental setup

The target plasmas in related shots are with the input NBI torque  $T_{NBI,E} \approx 1.1$  Nm, the normalized beta  $\beta_N \approx 1.8$ ,  $q_{95} \approx 3.7$ , and a similar ion and electron temperature  $T_i \approx T_e$ . An upper single null magnetic configuration is used as shown in Fig. 1(b). The upper divertor was upgraded with actively cooled ITER-like W/Cu mono-block plasma facing component previously in 2014.<sup>34</sup> Other parameters include the toroidal magnetic field strength  $B_T = 1.5$  T and the normalized pedestal electron collisionality  $\nu_{*,eped} \approx 0.5 - 0.8$ . The auxiliary heating power includes 2.5 MW neutral beam injection (NBI) and 1 MW lower hybrid current drive (LHCD). They are kept constant during the application of RMPs.

### B. Introduction of RMP coil system on EAST

In EAST, the RMP field is generated by an in-vessel coil system,<sup>33,35</sup> which has two up-down symmetric coil arrays at low field side (LFS) as shown in Fig. 1. Each array consists of eight coils evenly distributed along the toroidal direction ( $\Phi$ ) to generate RMP fields with  $n$  up to 4, and each coil has 4 turns. The definition of the toroidal angle  $\Phi = 0^\circ$  is the middle of port-A and port-P on EAST, which is also the toroidal angle of the center of the RMP coil  $U_1$  or  $L_1$ . The positive direction of  $\Phi$  is anticlockwise viewed from above. In each coil array, current in the  $k$ th coil can be written as

$$I(k) = \sum_n I_n \cos[n\phi(k) - \phi_n], \quad (1)$$

where  $\phi(k)$  is the toroidal angle of  $k$ th coil's center, and  $I_n$  and  $\phi_n$  are the amplitude and phase of the  $n$ th harmonic coils' current, respectively. Rotating field can be generated if  $\phi_n$  varies with time. Due to the design of power supply system of RMP coils in EAST, a combination of  $n = 2$  and  $n = 3$  harmonics in one coil array (upper or lower) cannot be produced in EAST. In this experiment, mixed  $n$  RMPs are set by employing  $n = 2$  harmonic of coil current in the upper array and  $n = 3$  one in the lower array. One example of coil current distributions is shown in Fig. 1(c).

### C. Modeling approach for magnetic footprint on a divertor during the application of RMPs

Three dimensional magnetic topology at plasma edge induced by RMPs causes non-axisymmetric heat and particle fluxes on the

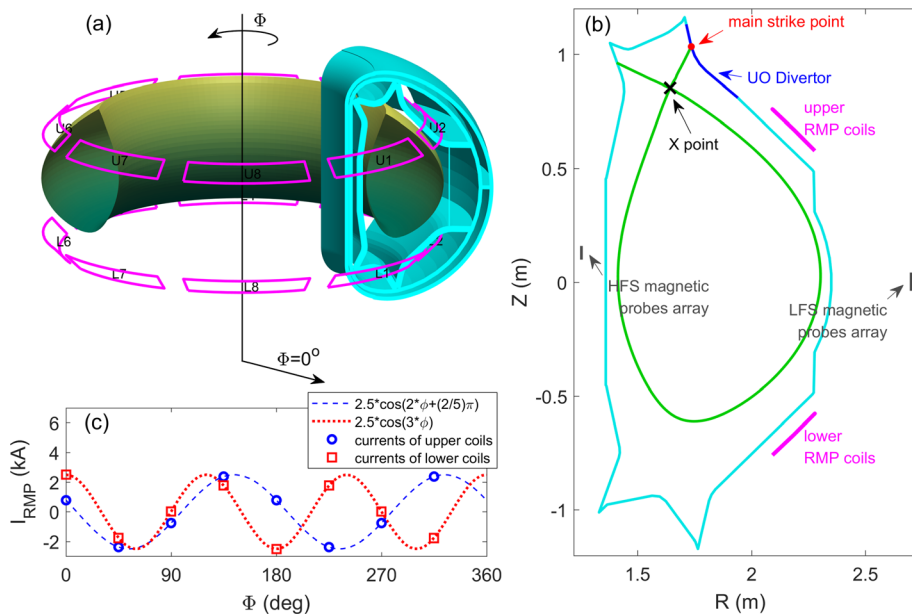


**FIG. 1.** (a) Three dimensional view of RMP coils (magenta saddle loops) together with the vacuum vessel (1/8 toroidal part, cyan layers) and plasma boundary (1/2 toroidal part, green surface) in EAST. (b) Two dimensional view of RMP coils (magenta segments) together with separatrix of an upper single null configuration (green solid line), strike points (red dots) on divertor plates (blue lines), and two toroidal-distributed magnetic probe arrays (dark gray segments) at high field side (HFS) and low field side (LFS) projected in a poloidal plane. (c) Coil current distribution for  $n=2$  (blue circles with dashed line) and  $n=3$  (red squares with dotted line) RMPs.

divertor target.<sup>20</sup> In the 3D configuration, patterns of divertor heat and particle fluxes are strongly correlated with the field line connection depth  $\rho_{min}$  at each point on the divertor target because particle and heat parallel transport along the perturbed field lines are orders of magnitudes higher than the cross field perpendicular ones. Here,  $\rho_{min}$  is defined as the radial position of the inner most magnetic flux surface that those magnetic field lines can connect with. Radial coordinate is chosen as  $\rho = \sqrt{\psi_{p,N}}$ , i.e., square root of the normalized poloidal magnetic flux with  $\psi_{p,N} = 1$ , the unperturbed separatrix. Profile of  $\rho_{min}$  on the divertor target indicates the pattern of magnetic footprint on the divertor target and hence links to the pattern of divertor fluxes. Profile of  $\rho_{min}$  in a poloidal plane (similar to the Poincaré plot of field line trajectory) is also a good indication for magnetic field topology. Therefore, a field line tracing code TOP2D<sup>36</sup> is employed for the modeling of  $\rho_{min}$  profile. The edge magnetic topology and footprint on the divertor target are used for comparison with divertor flux patterns during the application of RMPs in related analyses in this paper. Both vacuum and plasma response magnetic perturbations can be taken into account in TOP2D modeling.<sup>22</sup> In this study, RMPs with plasma response are modeled by the MARS-F code, in which a resistive single-fluid MHD model with a full toroidal geometry is employed.<sup>37–39</sup> Here, Spitzer resistivity and plasma toroidal rotation are used.

Figure 2 shows one example of modeled edge magnetic topology and footprint on the divertor induced by mixed  $n=2$  and 3 RMPs in the EAST discharge 79013 at 5 s using the TOP2D code.  $L$  is a measure of distance along the divertor plate to the main strike point where magnetic separatrix intersects with the divertor. A positive value of  $L$  is defined in an upward direction along the divertor. Profiles of  $\rho_{min}$  in a poloidal plane at  $\Phi = 80^\circ$  and on the upper outer divertor are shown in the colored contour plots in Fig. 2. Perturbed magnetic topology near the X point shows a clear lobe structure.<sup>19,40</sup> The pattern of the

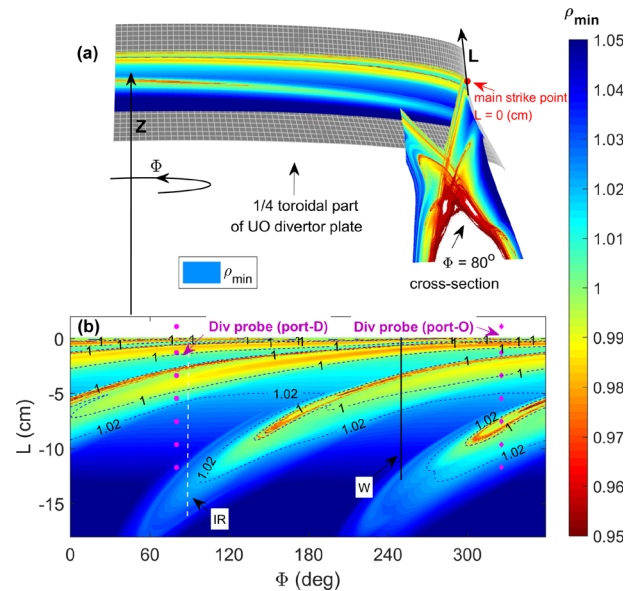


**FIG. 2.** Illustration of 3D magnetic topology and footprint pattern on the upper outer divertor under RMPs setting at 5 s in the EAST pulse 79013 modeled by the TOP2D code. (a) 2D view of the magnetic footprint pattern on the upper outer divertor plate (a quarter of the toroidal divertor plate) and the Poincaré plot of the edge magnetic field structure at a poloidal cross-section at  $\Phi = 80^\circ$ . (b) Projected 2D view of the magnetic footprint on the full upper outer divertor plate. Contour line of  $\rho_{min} = 1$  (blue dashed line) and  $\rho_{min} = 1.02$  (blue dotted-dashed line), positions of divertor Langmuir probes at post-D (magenta dots) and port-O (magenta diamonds), toroidal positions of a divertor tungsten (W) spectroscopy system (black line), and IR thermography (white dashed line) are marked.



magnetic footprint on the upper outer divertor shows a periodic change along the toroidal direction. The periodicity depends on the toroidal mode number of RMPs, and  $n = 2$  component dominates the pattern on the upper outer divertor and detailed discussion will be presented in Sec. IV B. This suggests the formation of toroidally localized steady state heat flux during RMP-ELM control.

For the convenience of making comparison between the field line penetration depth,  $1 - \rho_{min}$  is used to quantify the radial distance from  $\rho_{min}$  to the location of the unperturbed last closed flux surface or separatrix ( $\rho = 1$ ). As a result,  $1 - \rho_{min} > 0$  means that the field line can reach deep inside the plasma region relative to the unperturbed separatrix, while  $1 - \rho_{min} < 0$  means that the field line only travels in the so-called scrape-off layer outside the unperturbed separatrix. Therefore, the location of the divertor is expected to endure higher heat and particle flux with a deeper field line penetration depth, i.e., larger value of  $1 - \rho_{min}$ .

#### D. Main diagnostics for divertor flux measurement

Various diagnostics for particle and heat fluxes on the divertor at different toroidal positions are employed in this study. Recycling signal,  $D_{\alpha}$ , is generally used to indicate ELMs from filterscope diagnostic.<sup>41</sup> Divertor particle flux is measured using the saturated ion flux  $\Gamma_i$  by the divertor Langmuir probe arrays with a spatial resolution of 1.5–2 cm and a temporal resolution of 0.02 ms.<sup>42,43</sup> Two arrays of upper outer divertor probes located at port-D (toroidal angle  $\Phi = 80^\circ$ ) and port-O ( $\Phi = 327^\circ$ ) are used for measuring the saturated ion flux  $\Gamma_i$  to indicate non-axisymmetric particle flux on the divertor. Infrared (IR) thermography system is used to measure the temperature of the divertor target plate at  $\Phi = 88^\circ$ , and the heat flux profiles are calculated based on it.<sup>44,45</sup> A tungsten (W) spectroscopy system measuring an emission intensity of W I line at 400.9 nm on the upper outer divertor (at  $\Phi \approx 250^\circ$ ) with a spatial resolution of about 1.3 cm and a temporal resolution of 5 ms for investigating the W source sputtering was built on EAST.<sup>46</sup> It can also be used as a measure of divertor particle and heat fluxes. The locations of these diagnostics are marked in Fig. 2(b). In addition, five arrays of magnetic probes and saddle loops covering full toroidal positions are employed for the measurement of magnetic perturbation induced by plasma responses.<sup>47</sup> Positions of the two magnetic probe arrays used in this paper are shown in the poloidal plane in Fig. 1(b).

### III. ELM SUPPRESSION BY MIXED $n = 2$ AND 3 RMPS IN EAST

Limited by the maximal coil current, the use of mixed  $n$  RMPS will also reduce the possible amplitude of each  $n$  harmonic compared to single  $n$  RMPS cases, in which all of the RMP coils' currents can be used for that harmonic. Therefore, we have to demonstrate ELM suppression with mixed harmonic RMPS with a similar level of coil current for single  $n$  RMPS that achieved ELM suppression. In this section, ELM suppression without a drop of energy confinement is successfully demonstrated by using mixed  $n = 2$  and 3 RMPS in EAST. The control effects are compared with the single  $n$  harmonic cases. It will be shown that the  $n = 3$  harmonic plays the key role in accessing ELM suppression.

#### A. Demonstration of ELM suppression by mixed $n = 2$ and $n = 3$ RMPS in EAST

A promising example that ELM suppression achieved by RMPS with mixed static  $n = 2$  and  $n = 3$  harmonics, in EAST shot 79016, is shown in Fig. 3. Mixed  $n$  RMPS is set by employing  $n = 2$  harmonic of

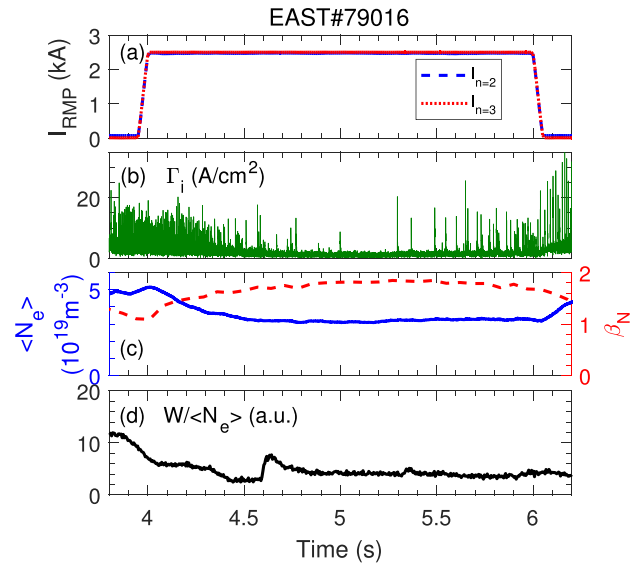


**FIG. 3.** ELM suppression using mixed  $n = 2$  and 3 RMPS in EAST pulse 79016. Temporal evolution of (a)  $n = 2$  (blue dashed solid) and 3 (red dotted line) RMP coil current, (b) saturated ion flux on the divertor indicating ELM crashes, (c) averaged plasma density (blue solid line) and the normalized plasma beta (red dashed line), and (d) tungsten (unresolved transition array (W-UTA) in 45–65 Å) emission intensity at the chord crossing plasma core, which is normalized to the density.

coil current in the upper array and  $n = 3$  one in the lower array. The amplitudes of coil currents for both  $n = 2$  and 3 harmonics are 2.5 kA and phases for  $n = 2$  and 3 are  $-2/5\pi$  and 0, respectively. Currents of RMP coils in shot 79016 have been shown in Fig. 1(c), and phase information is also stated in legends. The two phases of  $n = 2$  and  $n = 3$  harmonic were experimentally determined within the phase range achieved ELM suppression in the similar target plasma, shot 79013, which will be discussed in detail in Sec. IV. It is shown that ELM suppression is kept during RMP application from about 4.5 to 5.6 s with some remaining occasional events, as shown by  $\Gamma_i$  induced by ELMs.  $D_{\alpha}$  signal is not available in this shot. After 5.6 s, the ELM suppression is lost due to a minor increase in upper triangularity  $\Delta_{up}$ , which will be discussed later in III C. A strong density pump-out effect ( $\approx 36\%$  density drop) is observed during the RMP application, while  $\beta_N$  increases slightly during ELM suppression as shown in Fig. 3(c). Additionally, ELM suppression is achieved when density pump-out is close to saturation state and density is about  $3 \times 10^{19} \text{ m}^{-3}$ . This means the energy confinement is improved during ELM suppression, which is different from previous observations of strong energy confinement degradation with the  $n = 1$  or 2 RMPS applications<sup>12</sup> but is similar to that in the  $n = 4$  RMPS cases.<sup>16</sup> The tungsten concentration from the EUV system<sup>48,49</sup> is also significantly reduced after the application of RMPS as shown in Fig. 3(d), which is similar to our previous observations with single  $n$  RMPS.<sup>16</sup> This demonstrates as well a robust effect on the avoidance of tungsten accumulation in the plasma core using RMPS.

#### B. Compared to ELM suppression using single $n = 2$ and $n = 3$ RMPS in EAST

Figure 4 shows ELM control in another two shots 80845 with single  $n = 2$  RMPS and 80646 with single  $n = 3$  RMPS, respectively.

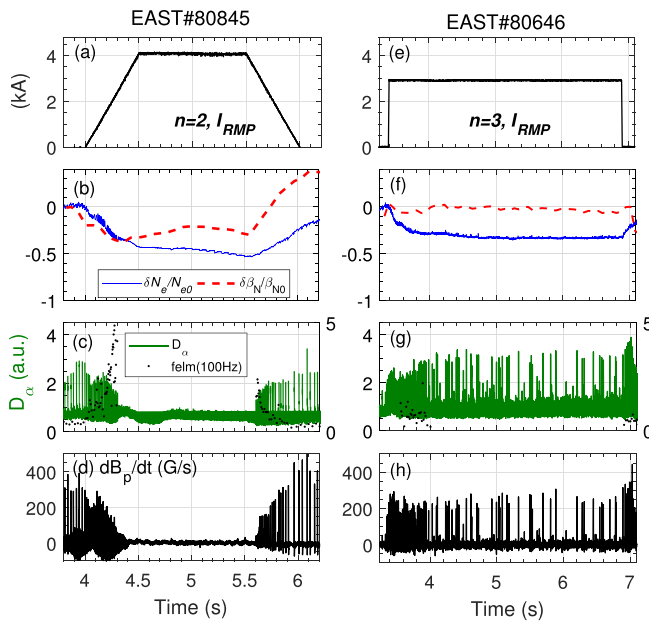


**FIG. 4.** ELMs control using single  $n=2$  and single  $n=3$  RMPs in EAST pulse 80 845 (a)–(c) and 80 646 (d)–(f), respectively. From top to bottom are the temporal evolution of (a and d) RMP coil current, (b and e) variation ratios of plasma density (blue solid line) and normalized plasma beta (red dashed line) compared to no RMP cases, (c and g)  $D_\alpha$  (green solid line) and ELM frequency (black dot) (d) and (h) Mirnov signal from magnetic probe.

Here, single  $n$  means that upper and lower coil arrays generate magnetic perturbations with the same toroidal number  $n$  and the same amplitude of coil current. In shot 80 845,  $n=2$  field is generated with  $\phi_{U,n=2} = 225^\circ$  and phase difference between upper and lower coils,  $d\phi_{UL} = 180^\circ$ . In shot 80 646,  $n=3$  field is generated with  $\phi_{U,n=3} = 0^\circ$  and  $d\phi_{UL} = 0^\circ$ . The spectra are all optimized for ELM control. Fully ELM suppression is achieved by single  $n=2$  RMPs in shot 80 845. The threshold coil current of  $n=2$  RMPs for ELM suppression is about 2.5 kA, above which a very robust suppression is achieved. A strong density pump-out effect with about 50% density drop is observed, and the energy drop is about 20%. In the  $n=3$  RMPs case, most of ELMs are suppressed with a coil current at around 2.9 kA, except some non-periodic ELMs appear occasionally in EAST pulse 80 646. This suggests that the suppression effect is not so robust as that in the mixed  $n$  case. In this experiment, 2.9 kA already the maximum current for  $n=3$  due to the limit of power supply. It could be possible that the marginal ELM suppression can be avoided with the upgrading power supply. Compared to the  $n=2$  RMP case, a weaker variation of plasma confinements caused by  $n=3$  RMP is observed, i.e., density drop is about 29%, while the normalized plasma beta maintains the same level. Therefore, there is no drop of energy confinement in the single  $n=3$  RMPs case, which is similar to the  $n=4$  RMPs case in EAST reported before.<sup>16</sup>

ELM suppression is achieved by  $n=2$  RMP with decreased confinements of both density and energy. Although just partial ELM suppression being achieved using  $n=3$  RMP, no obvious  $\beta_N$  drop is observed. A mixture of 2.5 kA  $n=2$  and 3 harmonics, discussed in Sec. III A, achieves more robust ELM suppression than the 2.9 kA

single  $n=3$  case, i.e., with much less and smaller remnant single ELMs and better energy confinement than the single  $n=2$  case.

### C. Understanding ELM suppression mechanism with mixed $n=2$ and $n=3$ RMPs

The corresponding RMP field strength modeled by the MARS-F code in the three cases is compared in Fig. 5. Edge islands' widths in different RMP cases are shown in (a) with current threshold for single  $n=2$  RMP ELM suppression of about 2.5 kA in shot 80 845, (b) 2.9 kA single  $n=3$  RMP in shot 80 646, and (c) 2.5 kA mixed  $n=2$  and  $n=3$  RMPs in shot 79 016. It is shown that the single  $n=2$  RMPs case in shot 80 845 has the strongest RMP field. It may explain the relatively robust ELM suppression effect observed in this case. From normalized  $\rho_t = 0.85$  ( $q \approx 3$ , near pedestal top) to 0.6 ( $q \approx 2$ , core), the  $n=2$  island widths at corresponding rational surfaces fall to 58.3% while 41.7% for  $n=3$  case. Thus, it is relatively a slow decay for  $n=2$  RMP case, which may result in strong influence on global confinement as well. The island widths have a faster decay from edge to core with the single  $n=3$  RMP. It means that the  $n=3$  harmonic influences the local area near the edge rather than the global plasma area.

Although both the  $n=2$  and 3 harmonics in the mixed  $n$  case are weaker than the single  $n$  harmonic cases, more components on rational surfaces are created, which may lower the required RMP strength to access ELM suppression. Resonances produced by mixed  $n$  RMP are strong in the pedestal region referring to  $0.87 \leq \text{normalized } \rho_t \leq 1$ , and the strength of resonances in core referring to normalized

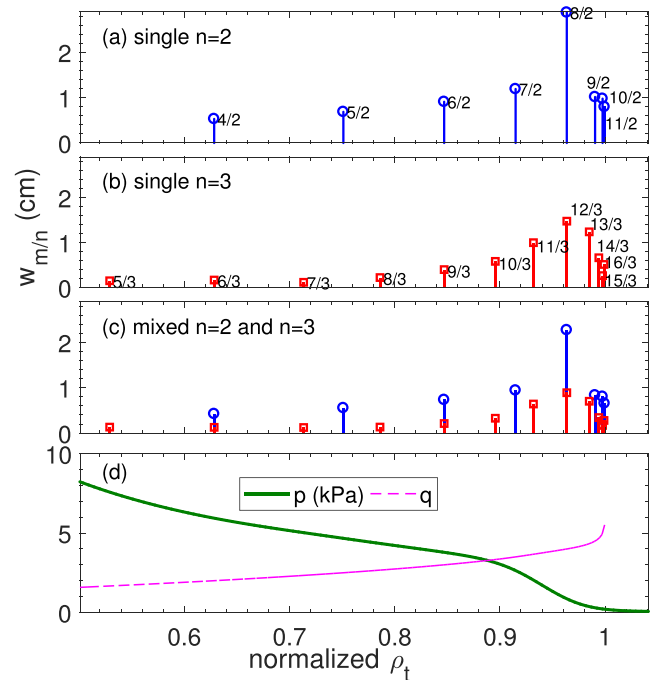


**FIG. 5.** Comparison of edge islands' widths between different RMP applications (a) with current threshold for single  $n=2$  RMP ELM suppression of about 2.5 kA in shot 80 845, (b) with 2.9 kA single  $n=3$  RMPs in shot 80 646, and (c) 2.5 kA mixed  $n=2$  and  $n=3$  RMPs in shot 79 016. Radial profiles of pressure and safety factor  $q$  are presented in (d).

$\rho_t < 0.87$  is weak. The two effects contribute to the ELM suppression access (although with some remnant single ELMs) and the energy confinement maintenance in using mixed  $n = 2$  and 3 RMPs for ELM suppression observed in shot 79 016.

Plasma responses measured from magnetic diagnostics show that the larger  $n = 3$  response is the key for transition from ELM mitigation to suppression. Fourier components of magnetic perturbations,  $\delta B_p$ , due to plasma response are measured by magnetic probes at both low field side and high field side as shown in Fig. 6. The subscript “p” denotes the poloidal component of the perturbed magnetic plasma response. During the transition from  $t = 4.3$  to 4.5 s,  $n = 3$   $\delta B_p$  increased at LFS by a ratio of 2, while  $\beta_N$  increased by a ratio of 1.05. Linear response with increase  $\beta_N$  is not enough to explain the significant increase in  $\delta B_p$ . At  $t \approx 4.35$  s, a stir-like change of density evolution can be distinguished in Figs. 6(b) and 6(c). Tungsten emission intensity normalized with density has also shown a similar stair-like change at  $t = 4.3$  s in Fig. 3. Evolutions of density and tungsten emission intensity are close to the saturation state before  $t = 4.3$  s and then

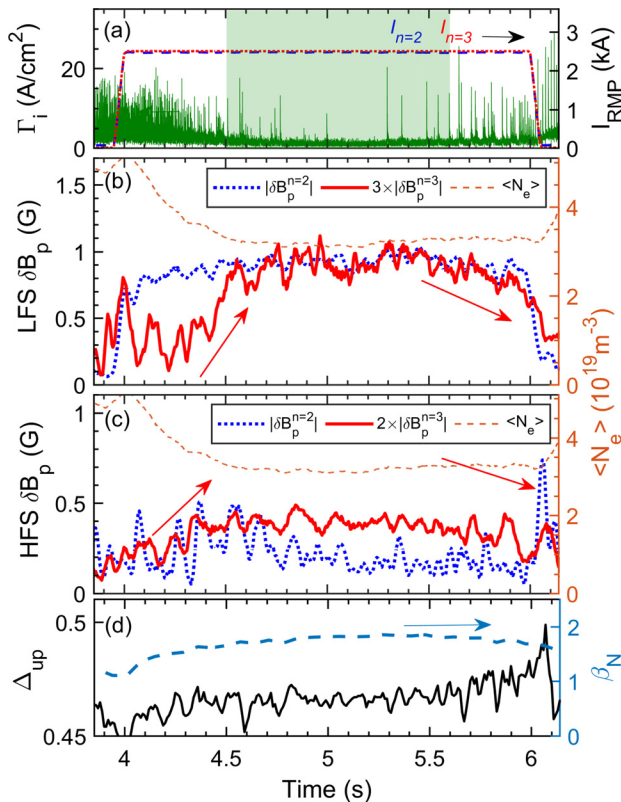


**FIG. 6.** Magnetic perturbation in the poloidal direction,  $\delta B_p$ , induced by plasma response to mixed  $n$  RMPs in EAST pulse 79 016. Temporal evolution of (a) saturated ion flux indicating ELM behavior and RMP coil current of  $n = 2$  and  $n = 3$  harmonics, amplitude of  $n = 2$  (blue dotted line) and  $n = 3$  (red solid line) Fourier components of magnetic perturbation induced by plasma response measured by low field side (LFS) magnetic probe array (b) and by high field side (HFS) magnetic probe array (c) and density evolution is also shown in (b) and (c). Amplitude changes of  $n = 3$  harmonic component are indicated by red arrows. (d) Temporal evolution of upper triangularity  $\Delta_{up}$  (solid black line) and the normalized plasma beta (grayish blue dashed line).

drop again until another saturation was achieved at  $t = 4.5$  s when most ELMs have been suppressed. Those evolutions did not follow a smooth change here.  $\beta_N$  increased from 1.2 to 1.7 due to the exhaust of tungsten impurity from the start time of RMP, which may also result in plasma response change. Magnetic responses consist of both linear response change due to equilibrium evolutions and non-linear process. Linear or non-linear response change from magnetic measurements needs to be confirmed by RMP current ramp-up with a small variation of equilibrium evolution in further experiment. Fast magnetic response change in a 10 ms time scale<sup>50</sup> cannot be distinguished here, which might be due to the long time transport scale physical process. ELM suppression is lost at  $t \approx 5.6$  s when  $n = 3$  component response decreases gradually to a lower level as shown in Fig. 6, which might be due to the unexpected slight drop of  $\beta_N$  or a minor increase in the upper triangularity  $\Delta_{up}$ .<sup>51</sup>

There is no obvious change in the  $n = 2$  harmonic of plasma response at the time entering or exiting ELM suppression. The enhancement of  $n = 3$  harmonic response plays the key role in accessing ELM suppression in the mixed harmonics RMP experiment. It can also explain the similarity of ELM control effects between the mixed harmonic experiments and the single  $n = 3$  RMP experiment.  $n = 3$  harmonic response changes to accessing ELM suppression were also observed but in a fast way in DIII-D mixed  $n$  RMP experiment; meanwhile,  $n = 2$  responses were linear with the applied  $n = 2$  harmonic.<sup>28</sup> Although no obvious change being detected in the evolution of  $n = 2$  plasma response, it may help the enhancement of  $n = 3$  harmonic via 3D effects on nearby rational surfaces or modifications to the rotation profile, which need further verification from both experiments and modeling.

#### IV. DYNAMICAL MOVEMENT OF THE SPLITTING PATTERNS OF DIVERTOR FLUX USING MIXED $n$ RMPs INCLUDING ROTATING $n = 2$ HARMONICS

The achievement of ELM suppression using fixed RMP field with mixed harmonics allows further investigation about the effect on divertor power load with rotating harmonics. In this experiment, the dynamical movement of the splitting lobes, which can avoid localized heat load accumulation on the divertor target, is achieved with rotating only  $n = 2$  harmonic and ELM suppression can be maintained in part of the phase range. Partial amplitude of the current work in an alternating mode rather than whole amplitude can ease mechanical stress.

##### A. Demonstration of divertor flux modification using mixed static $n = 3$ and rotating $n = 2$ RMPs

Figure 7 shows an example of dynamical ELM and divertor flux control using mixed  $n$  RMPs with a rotating  $n = 2$  harmonic current in the upper coils and a static  $n = 3$  harmonic current in the lower coils from 4 to 6 s in the EAST pulse 79 013. The amplitude of both  $n = 2$  and  $n = 3$  harmonics is 2.5 kA, and the  $n = 2$  harmonic is rotated for two periods, which results in a one period rotation of the whole footprint pattern on a divertor target induced by  $n = 2$  component. During the rotation, ELMs are mostly suppressed from 4.9 s to 5.5 s as shown by the shaded area in Fig. 7(a), about 60% of one rotating cycle. The other ELM mitigation periods and occasionally appeared single ELMs during ELM suppression indicate that the total RMP field strength is still marginal for accessing a robust ELM suppression state. ELM suppression achieved in part of the phase range might be due to other



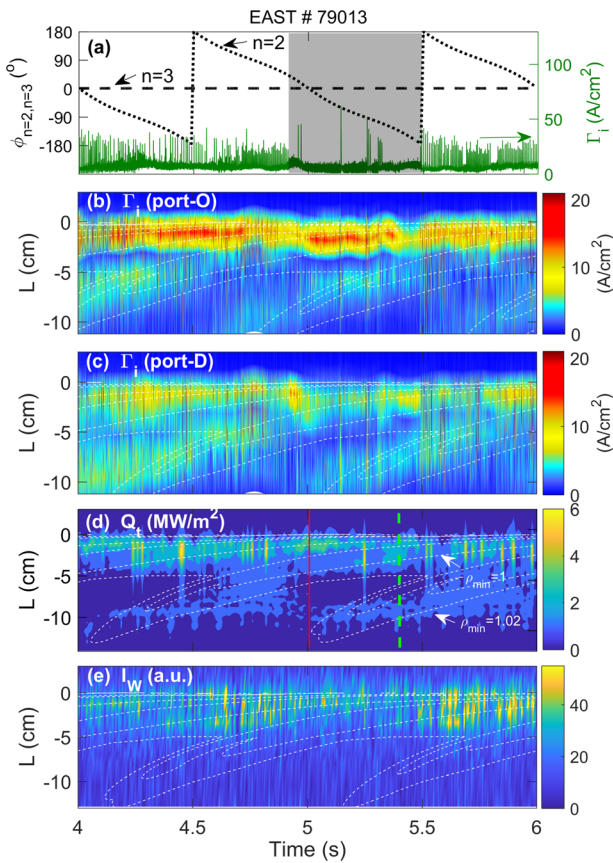


**FIG. 7.** Dynamical movement of the splitting patterns of divertor fluxes using mixed  $n$  RMPs with a rotating 2.5 kA  $n=2$  harmonic current in the upper coils and a 2.5 kA static  $n=3$  harmonic current in the lower coils in EAST pulse 79013. Temporal evolution of (a) the phase of  $n=2$  harmonic coil current (black dotted line), the phase of  $n=3$  harmonic coil current (black dashed line) and the saturated ion flux  $\Gamma_i$  on divertor (green solid line), and distributions of divertor fluxes along a vertical line on the divertor plate including the saturated ion flux measured by divertor probe arrays at (b) port-O (toroidal angle of  $327^\circ$ ) and (c) at port-D (toroidal angle of  $80^\circ$ ), (d) divertor heat flux based on IR thermography, and (e) W I line emission (400.9 nm) intensity. Contour lines for modeled  $\rho_{min}=1$  and 1.02 (white dashed lines) are superimposed on the divertor fluxes.

asymmetric factors, such as intrinsic error field and auxiliary heating, which needs further investigation.

Figure 7(b) and 7(c) shows the temporal evolution of the particle fluxes on the upper divertor during the application of RMPs. They are measured by two divertor probe arrays located on the upper outer divertor target at  $\phi = 80^\circ$  (port-D) and  $\phi = 327^\circ$  (port-O). The spiral splitting patterns can be distinguished, which vary periodically and keep in pace with the phase of  $n=2$  harmonic. The phase shift of the patterns of two arrays can be identified as expected, as the toroidal asymmetric characteristic of the strike line splitting pattern induced by the RMP field. During ELM suppression from 4.9 to 5.5 s, there is an effective poloidal shift of the steady state particle flux to the secondary lobes on the divertor target with the rotating  $n=2$  harmonic. It demonstrates the possibility of a dynamic control of divertor particle load

while maintaining ELM suppression with just one harmonic rotation in the mixed harmonics RMP field.

A similar effect on heat flux to the divertor is shown in Fig. 7(d). Profile of W I line emission (at 400.9 nm) on a divertor also shows a similar splitting of strike point during the application of RMPs in Fig. 7(e). Variation of the W I line emission intensity is localized at the near separatrix region. This suggests only the near separatrix on the divertor may be connected to hot plasma, which can give rise to W source sputtering. Effect of ELM burst on heat load and W source sputtering cannot be clearly identified because of the temporal resolution in these two diagnostics in this shot.

The patterns of the particle fluxes measured in both of these arrays and the heat flux measured by IR thermography match with the footprint pattern of  $\rho_{min}$  (white dashed lines) modeled by the TOP2D code as shown in Figs. 7(b)–7(e). Detailed comparison of profiles will be given in Subsection IV B.

## B. Modeling of magnetic footprint on the divertor target and comparison with observed divertor fluxes splitting

Modeling of magnetic topology and footprint on the divertor target under mixed  $n=2$  and  $n=3$  based on equilibrium and RMP settings are carried out for shot 79013 as shown in Fig. 2, which is based on experimental equilibrium and RMP settings. The  $n=2$  harmonic plays a dominant role in determining the shape of the magnetic footprint on the upper outer divertor, which can be identified from the feature of two periods in the footprint pattern on the whole toroidal divertor shown in Fig. 2(b). It is because the upper coil array generating the  $n=2$  field is closer to the upper outer divertor target and the  $n=2$  harmonic is stronger than the  $n=3$  harmonic as shown in Fig. 5. A detailed comparison of the modeling results with the observations will be discussed in the following.

Particle flux and heat flux profiles at two different time slices,  $t=5.0$  and  $5.4$  s, are both compared with the modeled field line penetration depth  $1-\rho_{min}$  as shown in Figs. 8 and 9, respectively. Each modeling is made according to the real coil configurations of the two time slices, i.e., with the phase of  $n=2$  harmonic  $\phi_{n=2}$  equals  $0^\circ$  and  $215^\circ$ , respectively. The toroidal angle of  $\rho_{min}$  profile is chosen according to the toroidal angle of each diagnostic. The particle flux (averaged over 0.5 ms) is measured by the divertor probe array at port-D [marked on Fig. 2(b)]. Due to limited spatial resolution of the divertor probes, the two modeling peaks ( $L \approx -1$  and  $L \approx -4$  cm) of the  $1-\rho_{min}$  profile at  $t=5.0$  s cannot be distinguished from particle flux, which looks like a broadened main peak at  $L \in [-6,0]$  cm rather than two flux peaks. However, the difference of two particle flux profiles ( $t=5$  and  $t=5.4$  s) at  $L \approx -4$  cm is evident due to different depths of magnetic field lines. As a result, the contribution to the second peak at  $t=5.0$  s from modeling the field line penetration depth changes induced by the RMPs can be deduced. The positions of the secondary peaks,  $L \approx -4$  cm at  $t=5.0$  s and  $L \approx -8$  cm at  $t=5.4$  s, are obviously different between the two time slices. The shift of the secondary peak positions of the two time slices is consistent with the shift of far SOL peaks in  $1-\rho_{min}$  profiles. It means there is an effective dynamical movement of the particle flux especially for additional flux peaks by the rotation of  $n=2$  harmonic with fixed  $n=3$  harmonic. With such toroidal and poloidal variations of the splitting lobes on the divertor target, local particle flux accumulation could be alleviated.



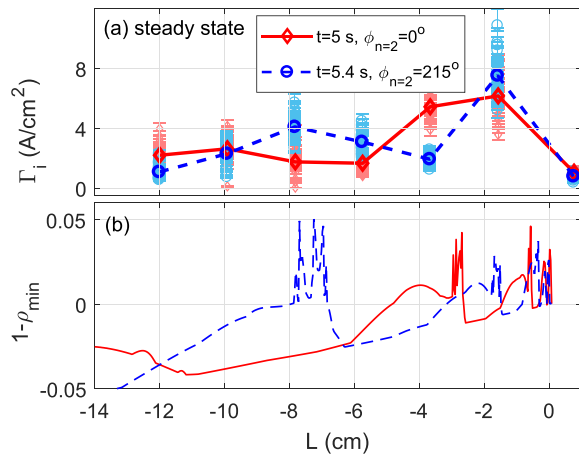


**FIG. 8.** Comparison of profiles of (a) steady state particle flux averaged over 25 time slices measured by divertor probe arrays at port-D along with raw data of 25 time slices and (b) the modeled penetration depth of magnetic field lines  $1-\rho_{min}$  along a vertical line on the upper outer divertor at two time slices  $t \approx 5.0$  ( $\phi_{n=2} = 0^\circ$ , red solid lines) and  $t \approx 5.4$  s ( $\phi_{n=2} = 215^\circ$ , blue dashed lines), respectively.

The heat flux profiles are measured by IR thermography. Each profile is time averaged over 50 ms including five time slices around  $t=5.0$  or  $5.4$  s during ELM suppression. At  $t=5.0$  s, the small peak near  $L=-4$  cm is consistent with the peak on the modeled  $1-\rho_{min}$  profile. Compared to the heat flux profile at  $t=5.0$  s, the increases of heat flux near  $L=-3$  cm and  $L=-9$  at  $t=5.4$  s agree with the peaks in the modeled  $1-\rho_{min}$  profile. It is also consistent with the larger value of  $1-\rho_{min}$  at  $L=-3$  and  $-9$  cm of the modeled profiles. In Fig. 9, 1~2 cm shift distinguished between peak positions of heat flux

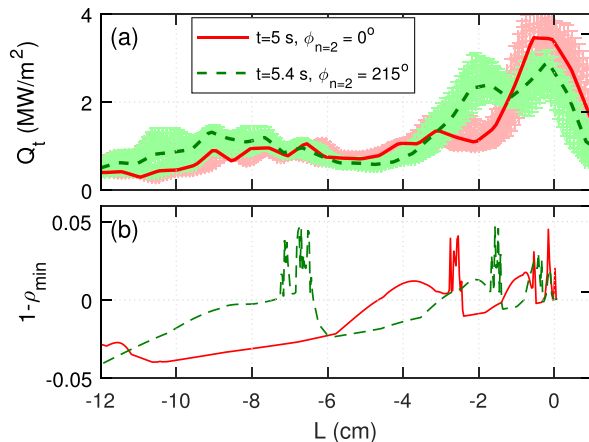


**FIG. 9.** Comparison of profiles of (a) divertor heat flux averaged over 5 time slices along with raw data of 5 time slices and (b) the modeled penetration depth of magnetic field lines  $1-\rho_{min}$  along a vertical line on the upper outer divertor at  $t=5$  ( $\phi_{n=2} = 0^\circ$ , red solid line) and  $t=5.4$  s ( $\phi_{n=2} = 215^\circ$ , green dashed line), respectively.

and respective  $1-\rho_{min}$  profile might be due to different edge diffusions of heat and particle flux, which will be considered to be introduced in modeling in future and uncertainty of main strike point position from equilibrium calculation. These features indicate that the rotation of the  $n=2$  harmonic, only being part of the whole RMP field, can also make a dynamic magnetic footprint and thus effectively modify the heat flux on the divertor target. Although ELM suppression is achieved during only part of a full rotation period of the  $n=2$  harmonic in shot 79 013, the steady state particle and heat fluxes are effectively modified on part of the divertor target with the  $n=2$  harmonic rotation combined with fixed  $n=3$  harmonic. Such dynamical control can be further optimized with more robust ELM suppression, which will be better for alleviating local particle and heat accumulation compared to a static RMP field.

### C. Effects on transient divertor flux during ELM mitigation

During RMP application, the transient particle flux profile induced by the ELM crash also shows a splitting pattern and the toroidal shift of the pattern seems also consistent with the prediction by numerical modeling of the phase shift of the magnetic footprint. A zoom in of Figs. 7(c) and 7(a) is shown in Figs. 10(a) and 10(b), which contains several clear ELM bursts. Two profiles of the ELM induced transient particle flux, at  $t=4.652$  s with  $\phi_{n=2} \approx 120^\circ$  and  $t=4.247$  s with  $\phi_{n=2} \approx 270^\circ$ , are compared with the modeled magnetic field line penetration depth  $1-\rho_{min}$  in Figs. 10(c) and 10(d). It seems the position of the secondary particle flux peak also agrees well with the

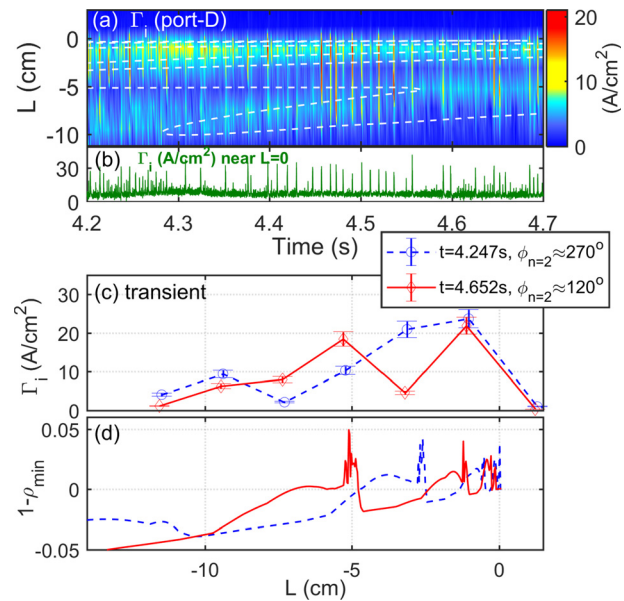


**FIG. 10.** Observation of splitting transient particle flux during ELM crashes. Temporal evolution of (a) the particle flux profile on the divertor and (b) the particle flux near the main strike point ( $L=0$  cm) measured by divertor Langmuir probes at port-D in ELM mitigation phase. Comparison of (c) ELM-induced transient particle flux profiles at  $t \approx 4.247$  (blue dashed lines) and  $t \approx 4.652$  s (red solid lines) with (d) the modeled penetration depth of magnetic field lines  $1-\rho_{min}$  at the corresponding time slices.

$1 - \rho_{min}$  peak predicted by modeling. It means the transient particle flux induced by ELMs also shows a spiral pattern with a toroidal asymmetry and the phase shift keeps pace with the rotating  $n = 2$  harmonic. This observation is similar to the splitting distribution of transient heat flux by mitigated ELMs under  $n = 2$  RMPs in JET.<sup>52</sup> This phenomenon might be due to locking of ELM crash phase into the applied RMP field<sup>53</sup> or particle transport through the reformed low  $n$  magnetic field line induced by the applied RMP at the SOL region. In this shot, the analysis and observation of ELM induced transient particle flux are quite superficial due to the limited spatial resolution of the divertor probe array and the limited temporal resolution of the IR thermography. It is worth making further investigation on the mechanism for the effect of RMP field on ELM induced transient heat fluxes.

## V. SUMMARY AND CONCLUSIONS

In summary, we present a new demonstration of the integrated control of ELMs and steady state divertor fluxes using RMPs with a mixture of static  $n = 3$  and rotating  $n = 2$  toroidal harmonics in the EAST tokamak. This is achieved in a target plasma close to the ITER high fusion gain operation equivalent low input torque, high normalized beta, low edge safety factor, and tungsten divertor.

The stored energy during ELM suppression achieved with a mixture of 2.5 kA low  $n$  harmonic ( $n = 2$ ) and 2.5 kA high  $n$  harmonic ( $n = 3$ ) RMPs is better compared to that during ELM suppression by single low  $n$  harmonic ( $n = 2$ ) RMP with 2.5 kA current. The improved energy confinement is similar to the ELM suppression achieved with high  $n$  ( $n = 3$  or 4) RMPs.<sup>17</sup> The mixture of 2.5 kA  $n = 2$  and 3 harmonics achieves more robust ELM suppression than the 2.9 kA single  $n = 3$  case, i.e., with much less remnant single ELMs. The tungsten concentration is also effectively reduced during the application of mixed  $n$  RMPs.

The plasma response measurement on EAST reveals that larger  $n = 3$  plasma response plays a key role to access ELM suppression with mixed  $n = 2$  and  $n = 3$  RMPs. Density pump-out and larger  $\beta_N$  contribute to enhanced  $n = 3$  plasma response. During transition from ELM mitigation to suppression, both evolutions of density and tungsten emission intensity normalized with density have also shown a stair-like drop, which might suggest a nonlinear process. The common feature with DIII-D mixed  $n$  RMP experiments is that ELM suppression is related to a change of  $n = 3$  magnetic response and  $n = 2$  response follow linear change with the applied  $n = 2$  RMP field.<sup>28</sup>

The effective dynamical movement of the splitting pattern of both the transient (ELMs) particle fluxes and steady state particle/heat fluxes is achieved using mixed harmonics RMPs with a rotating  $n = 2$  harmonic and a fixed  $n = 3$  harmonic. ELM suppression over 60% cycle of one period rotating  $n = 2$  RMPs is achieved. The toroidally varying steady state divertor particle and heat fluxes can be moved by the rotating  $n = 2$  harmonic during ELM suppression. In addition, it is also interesting to observe that the transient particle flux induced by ELM crashes during RMP application in EAST is locked to the phase of  $n = 2$  harmonic. The mixed harmonic RMPs have different realizations. Despite in EAST using upper  $n = 2$  and lower  $n = 3$  combinations, there are other schemes, such as by combining low and high  $n$  harmonics in both lower and upper arrays and changing their ratio or phases, the feature of the splitting magnetic footprint, such as the number of lobes and the shape of each lobe, is affected by the ratio between the harmonics as described in Ref. 25.

Similar to the results in DIII-D, there is no increase in the required coil current in the mixed harmonic RMPs case compared to that of the single harmonic RMPs case. The change is only in the RMP coil phase space employing different combinations. These results further confirm the effectiveness of mixed harmonic RMPs in suppressing ELMs and dynamical controlling the divertor particle and heat fluxes.

## ACKNOWLEDGMENTS

This work was supported by the National Key R&D Program of China under Grant Nos. 2017YFE0301100 and 2017YFE0301300, the National Natural Science Foundation of China under Grant Nos. 12005261, 11875292, and 12105323, the Natural Science Foundation of Anhui Province under Grant No. 2208085J39, the Science Foundation of Institute of Plasma Physics, Chinese Academy of Sciences Grant No. DSJJ-2020-05, and also the U.S. DOE Under Grant Nos. DE-SC0020298 and DE-SC0021968.

## AUTHOR DECLARATIONS

### Conflict of Interest

The authors have no conflicts to disclose.

## Author Contributions

**Qun Ma:** conceptualization (lead); data curation (lead); formal analysis (equal); investigation (lead); methodology (equal); visualization (lead); and writing—original draft (lead). **Youwen Sun:** conceptualization (equal); formal analysis (equal); funding acquisition (equal); investigation (equal); project administration (equal); supervision (equal); and writing—review and editing (equal). **Manni Jia:** conceptualization (equal); formal analysis (equal); and writing—review and editing (equal). **Shuai Gu:** conceptualization (equal); formal analysis (equal); and writing—review and editing (equal). **Xuemin Wu:** data curation (equal) and software (equal). **Pengcheng Xie:** data curation (equal) and software (equal). **Carlos Paz-Soldan:** funding acquisition (equal) and writing—review and editing (equal). **Yunfeng Liang:** conceptualization (equal). **Fangchuan Zhong:** conceptualization (equal) and writing—review and editing (equal). **Liang Wang:** data curation (equal). **Fang Ding:** data curation (equal) and writing—review and editing (equal). **Bin Zhang:** data curation (equal). **Tonghui Shi:** data curation (equal). **Biao Shen:** data curation (equal). **Huihui Wang:** conceptualization (equal) and formal analysis (equal). **Ling Zhang:** data curation (equal) and writing—review and editing (equal). **Yumin Wang:** data curation (equal). **Qing Zang:** data curation (equal). **Yingying Li:** data curation (equal). **Yueqiang Liu:** software (equal). **Baonian Wan:** conceptualization (equal).

## DATA AVAILABILITY

The data that support the findings of this study are available from the corresponding author upon reasonable request.

## REFERENCES

- Wagner, G., Becker, K., Behringer, D., Campbell, A., Eberhagen, W., Engelhardt, G., Fussmann, O., Gehre, J., Gernhardt, G., v Gierke, G., Haas, M., Huang, F., Karger, M., Keilhacker, O., Klüber, M., Kornherr, K., Lackner, G., Lisitano, G., G. Lister, H. M. Mayer, D. Meisel, E. R. Müller, H. Murmann, H. Niedermeyer, W. Poschenrieder, H. Rapp, H. Röhr, F. Schneider, G. Siller, E.

- Speth, A. Stäbler, K. H. Steuer, G. Venus, O. Vollmer, and Z. Yü, "Regime of improved confinement and high beta in neutral-beam-heated divertor discharges of the ASDEX tokamak," *Phys. Rev. Lett.* **49**, 1408–1412 (1982).
- <sup>2</sup>H. Zohm, "Edge localized modes (ELMs)," *Plasma Phys. Controlled Fusion* **38**, 105–128 (1996).
- <sup>3</sup>See <http://www.iter.org> for an introduction to ITER project's goals, history, organization, location *et al.*
- <sup>4</sup>A. Loarte, G. Saibene, R. Sartori, D. Campbell, M. Becoulet, L. Horton, T. Eich, A. Herrmann, G. Matthews, N. Asakura, A. Chanin, A. Leonard, G. Porter, G. Federici, G. Janeschitz, M. Shimada, and M. Sugihara, "Characteristics of type I ELM energy and particle losses in existing devices and their extrapolation to ITER," *Plasma Phys. Controlled Fusion* **45**, 1549–1569 (2003).
- <sup>5</sup>A. Loarte, B. Lipschultz, A. Kukushkin, G. Matthews, P. Stangeby, N. Asakura, G. Counsell, G. Federici, A. Kallenbach, K. Krieger, A. Mahdavi, V. Philipps, D. Reiter, J. Roth, J. Strachan, D. Whyte, R. Doerner, T. Eich, W. Fundamenski, A. Herrmann, M. Fenstermacher, P. Ghendrih, M. Groth, A. Kirschner, S. Konoshima, B. LaBombard, P. Lang, A. Leonard, P. Monier-Garbet, R. Neu, H. Pacher, B. Pegourie, R. Pitts, S. Takamura, J. Terry, E. Tsitrone, and ITPA Scrape-off Layer and Divertor Physics Topical Group, "Chapter 4: Power and particle control," *Nucl. Fusion* **47**, S203–S263 (2007).
- <sup>6</sup>T. Eich, B. Sieglin, A. Thornton, M. Faitsch, A. Kirk, A. Herrmann, W. Suttrop, JET contributors, MST contributors, and ASDEX Upgrade and MAST teams, "ELM divertor peak energy fluence scaling to ITER with data from jet, mast and ASDEX upgrade," in Proceedings of the 22nd International Conference on Plasma Surface Interactions, 2016, [*Nucl. Mater. Energy* **12**, 84–90 (2017)].
- <sup>7</sup>R. Hawryluk, D. Campbell, G. Janeschitz, P. Thomas, R. Albanese, R. Ambrosino, C. Bachmann, L. Baylor, M. Becoulet, I. Benfatto, J. Bialek, A. Boozer, A. Brooks, R. Budny, T. Casper, M. Cavinato, J.-J. Cordier, V. Chuyanov, E. Doyle, T. Evans, G. Federici, M. Fenstermacher, H. Fujieda, K. G'Al, A. Garofalo, L. Garzotti, D. Gates, Y. Gribov, P. Heitzenroeder, T. Hender, N. Holtkamp, D. Humphreys, I. Hutchinson, K. Ioki, J. Johner, G. Johnson, Y. Kamada, A. Kavin, C. Kessel, R. Khayrutdinov, G. Kramer, A. Kukushkin, K. Lackner, I. Landman, P. Lang, Y. Liang, J. Linke, B. Lipschultz, A. Loarte, G. Loesser, C. Lowry, T. Luce, V. Lukash, S. Maruyama, M. Mattei, J. Menard, M. Merola, A. Mineev, N. Mitchell, E. Nardon, R. Nazikian, B. Nelson, C. Neumeyer, J.-K. Park, R. Pearce, R. Pitts, A. Polevoi, A. Portone, M. Okabayashi, P. Rebut, V. Riccardo, J. Roth, S. Sabbagh, G. Saibene, G. Sannazzaro, M. Schaffer, M. Shimada, A. Sen, A. Sips, C. Skinner, P. Snyder, R. Stambaugh, E. Strait, M. Sugihara, E. Tsitrone, J. Urano, M. Valovic, M. Wade, J. Wesley, R. White, D. Whyte, S. Wu, M. Wykes, and L. Zakharov, "Principal physics developments evaluated in the ITER design review," *Nucl. Fusion* **49**, 065012 (2009).
- <sup>8</sup>J. Gunn, S. Carpentier-Chouchana, R. Dejarnac, F. Escourbiac, T. Hirai, M. Komm, A. Kukushkin, S. Panayotis, and R. Pitts, "Ion orbit modelling of elm heat loads on ITER divertor vertical targets," in Proceedings of the 22nd International Conference on Plasma Surface Interactions, 2016, [*Nucl. Mater. Energy* **12**, 75–83 (2017)].
- <sup>9</sup>T. E. Evans, R. A. Moyer, P. R. Thomas, J. G. Watkins, T. H. Osborne, J. A. Boedo, E. J. Doyle, M. E. Fenstermacher, K. H. Finken, R. J. Groebner, M. Groth, J. H. Harris, R. J. La Haye, C. J. Lasnier, S. Masuzaki, N. Ohya, D. G. Pretty, T. L. Rhodes, H. Reimerdes, D. L. Rudakov, M. J. Schaffer, G. Wang, and L. Zeng, "Suppression of large edge-localized modes in high-confinement DIII-D plasmas with a stochastic magnetic boundary," *Phys. Rev. Lett.* **92**, 235003 (2004).
- <sup>10</sup>T. E. Evans, R. A. Moyer, K. H. Burrell, M. E. Fenstermacher, I. Joseph, A. W. Leonard, T. H. Osborne, G. D. Porter, M. J. Schaffer, and P. B. Snyder, "Edge stability and transport control with resonant magnetic perturbations in collisionless tokamak plasmas," *Nat. Phys.* **2**, 419–423 (2006).
- <sup>11</sup>Y. M. Jeon, J.-K. Park, S. W. Yoon, W. H. Ko, S. G. Lee, K. D. Lee, G. S. Yun, Y. U. Nam, W. C. Kim, J.-G. Kwak, K. S. Lee, H. K. Kim, and H. L. Yang (KSTAR Team), "Suppression of edge localized modes in high-confinement KSTAR plasmas by nonaxisymmetric magnetic perturbations," *Phys. Rev. Lett.* **109**, 035004 (2012).
- <sup>12</sup>Y. Sun, Y. Liang, Y. Q. Liu, S. Gu, X. Yang, W. Guo, T. Shi, M. Jia, L. Wang, B. Lyu, C. Zhou, A. Liu, Q. Zang, H. Liu, N. Chu, H. H. Wang, T. Zhang, J. Qian, L. Xu, K. He, D. Chen, B. Shen, X. Gong, X. Ji, S. Wang, M. Qi, Y. Song, Q. Yuan, Z. Sheng, G. Gao, P. Fu, and B. Wan, "Nonlinear transition from mitigation to suppression of the edge localized mode with resonant magnetic perturbations in the EAST tokamak," *Phys. Rev. Lett.* **117**, 115001 (2016).
- <sup>13</sup>W. Suttrop, A. Kirk, V. Bobkov, M. Cavedon, M. Dunne, R. McDermott, H. Meyer, R. Nazikian, C. Paz-Soldan, D. Ryan, E. Viezzer, and M. Willensdorfer, the ASDEX Upgrade, and MST1 Teams, "Experimental conditions to suppress edge localised modes by magnetic perturbations in the ASDEX Upgrade tokamak," *Nucl. Fusion* **58**, 096031 (2018).
- <sup>14</sup>Y. Liang, H. Koslowski, P. Thomas, E. Nardon, S. Jachmich, A. Alfier, G. Arnoux, Y. Baranov, M. Becoulet, M. Beurskens, R. Coelho, T. Eich, E. D. L. Luna, W. Fundamenski, S. Gerasimov, C. Giroud, M. P. Gryaznevich, D. Harting, A. Huber, A. Kreter, L. Moreira, V. Parail, S. Pinches, S. Saarelma, O. Schmitz, and JET-EFDA contributors, "Active control of type-I edge localized modes with  $n = 1$  and  $n = 2$  fields on JET," *Nucl. Fusion* **50**, 025013 (2010).
- <sup>15</sup>A. Kirk, E. Nardon, R. Akers, M. Becoulet, G. D. Temmerman, B. Dudson, B. Hnat, Y. Liu, R. Martin, P. Tamain, D. Taylor, and the MAST team, "Resonant magnetic perturbation experiments on MAST using external and internal coils for ELM control," *Nucl. Fusion* **50**, 034008 (2010).
- <sup>16</sup>Y. Sun, Q. Ma, M. Jia, S. Gu, A. Loarte, Y. Liang, Y. Liu, C. Paz-Soldan, X. Wu, P. Xie, C. Ye, H. Wang, J. Zhao, W. Guo, K. He, Y. Li, G. Li, H. Liu, J. Qian, H. Sheng, T. Shi, Y. Wang, D. Weisberg, B. Wan, Q. Zang, L. Zeng, B. Zhang, L. Zhang, T. Zhang, C. Zhou, and E. Contributors, "First demonstration of full ELM suppression in low input torque plasmas to support ITER research plan using  $n = 4$  RMP in EAST," *Nucl. Fusion* **61**, 106037 (2021).
- <sup>17</sup>M. Jia, A. Loarte, Y. Sun, Q. Ma, X. Wu, P. Xie, S. Gu, J. Hou, K. He, G. Li, K. Li, Y. Li, Y. Liang, C. Paz-Soldan, T. Shi, B. Shen, B. Wan, H. Wang, L. Wang, Y. Wang, J. Xu, S. Xu, Z. Yang, Q. Zang, B. Zhang, J. Zhang, L. Zhang, and G. Zuo, "Integrated ELM and divertor power flux control using RMPs with low input torque in EAST in support of the ITER research plan," *Nucl. Fusion* **61**, 106023 (2021).
- <sup>18</sup>A. Loarte, G. Huijsmans, S. Futatani, L. Baylor, T. Evans, D. M. Orlov, O. Schmitz, M. Becoulet, P. Cahyna, Y. Gribov, A. Kavin, A. S. Naik, D. Campbell, T. Casper, E. Daly, H. Frerichs, A. Kirschner, R. Laengner, S. Lisgo, R. Pitts, G. Saibene, and A. Wingen, "Progress on the application of ELM control schemes to ITER scenarios from the non-active phase to DT operation," *Nucl. Fusion* **54**, 033007 (2014).
- <sup>19</sup>A. Kirk, J. Harrison, Y. Liu, E. Nardon, I. T. Chapman, and P. Denner (the MAST Team), "Observation of lobes near the x point in resonant magnetic perturbation experiments on MAST," *Phys. Rev. Lett.* **108**, 255003 (2012).
- <sup>20</sup>M. Jakubowski, T. Evans, M. Fenstermacher, M. Groth, C. Lasnier, A. Leonard, O. Schmitz, J. Watkins, T. Eich, W. Fundamenski, R. Moyer, R. Wolf, L. Baylor, J. Boedo, K. Burrell, H. Frerichs, J. deGrassie, P. Gohil, I. Joseph, S. Mordijck, M. Lehnen, C. Petty, R. Pinsker, D. Reiter, T. Rhodes, U. Samm, M. Schaffer, P. Snyder, H. Stoschus, T. Osborne, B. Unterberg, E. Unterberg, and W. West, "Overview of the results on divertor heat loads in RMP controlled H-mode plasmas on DIII-D," *Nucl. Fusion* **49**, 095013 (2009).
- <sup>21</sup>A. Thornton, A. Kirk, P. Cahyna, I. Chapman, G. Fishpool, J. Harrison, Y. Liu, L. Kripner, and M. Peterka, "ELM mitigation via rotating resonant magnetic perturbations on MAST," *J. Nucl. Mater.* **463**, 723–726 (2015).
- <sup>22</sup>M. Jia, Y. Sun, Y. Liang, L. Wang, J. Xu, S. Gu, B. Lyu, H. Wang, X. Yang, F. Zhong, N. Chu, W. Feng, K. He, Y. Liu, J. Qian, T. Shi, and B. Shen, "Control of three dimensional particle flux to divertor using rotating RMP in the EAST tokamak," *Nucl. Fusion* **58**, 046015 (2018).
- <sup>23</sup>M. Faitsch, B. Sieglin, T. Eich, A. Herrmann, W. Suttrop, and ASDEX Upgrade Team, "Divertor heat load in ASDEX Upgrade I-mode in presence of external magnetic perturbation," *Plasma Phys. Controlled Fusion* **59**, 095006 (2017).
- <sup>24</sup>S. Munaretto, D. Orlov, C. Paz-Soldan, I. Bykov, C. Lasnier, B. Lyons, and H. Wang, "Controlling the size of non-axisymmetric magnetic footprints using resonant magnetic perturbations," *Nucl. Fusion* **62**, 026018 (2021).
- <sup>25</sup>M. Jia, Y. Sun, C. Paz-Soldan, R. Nazikian, S. Gu, Y. Q. Liu, T. Abrams, I. Bykov, L. Cui, T. Evans, A. Garofalo, W. Guo, X. Gong, C. Lasnier, N. C. Logan, M. Makowski, D. Orlov, and H. H. Wang, "Dynamic divertor control using resonant mixed toroidal harmonic magnetic fields during ELM suppression in DIII-D," *Phys. Plasmas* **25**, 056102 (2018).
- <sup>26</sup>Y. Sun, S. Gu, M. Jia, Q. Ma, H. Wang, W. Guo, X. Gong, T. Shi, C. Paz-Soldan, Y. Liu, T. Abrams, T. Evans, A. Garofalo, S. Munaretto, R. Nazikian, L. Cui, N. Logan, D. Bykov, I. Orlov, M. Lasnier, and C. Makowski, "Dynamic ELM and divertor control using mixed toroidal harmonic resonant magnetic



- perturbations in DIII-D and EAST,” in *2018 IAEA Fusion Energy Conference Gandhinagar, India, October 22–27, 2018* (American Physical Society, 2018), pp. EX/7–2.
- <sup>27</sup>D. Orlov, R. Moyer, T. Evans, C. Paz-Soldan, N. Ferraro, R. Nazikian, J. deGrassie, B. Grierson, D. Eldon, M. Fenstermacher, J. King, N. Logan, M. Lanctot, R. Maingi, P. Snyder, E. Strait, and A. Wingen, “Suppression of type-I ELMs with reduced RMP coil set on DIII-D,” *Nucl. Fusion* **56**, 036020 (2016).
  - <sup>28</sup>S. Gu, Y. Sun, C. Paz-Soldan, R. Nazikian, M. Jia, H. Wang, W. Guo, Y. Liu, T. Abrams, L. Cui, T. Evans, A. Garofalo, X. Gong, N. Logan, S. Munaretto, D. Orlov, and T. Shi, “Edge localized mode suppression and plasma response using mixed toroidal harmonic resonant magnetic perturbations in DIII-D,” *Nucl. Fusion* **59**, 026012 (2019).
  - <sup>29</sup>A. C. C. Sips, G. Giruzzi, S. Ide, C. Kessel, T. C. Luce, J. A. Snipes, and J. K. Stober, “Progress in preparing scenarios for operation of the international thermonuclear experimental reactor,” *Phys. Plasmas* **22**, 021804 (2015).
  - <sup>30</sup>R. A. Moyer, C. Paz-Soldan, R. Nazikian, D. M. Orlov, N. M. Ferraro, B. A. Grierson, M. Knölker, B. C. Lyons, G. R. McKee, T. H. Osborne, T. L. Rhodes, O. Meneghini, S. Smith, T. E. Evans, M. E. Fenstermacher, R. J. Groebner, J. M. Hanson, R. J. La Haye, T. C. Luce, S. Mordijck, W. M. Solomon, F. Turco, Z. Yan, and L. Zeng, “Validation of the model for ELM suppression with 3D magnetic fields using low torque ITER baseline scenario discharges in DIII-D,” *Phys. Plasmas* **24**, 102501 (2017).
  - <sup>31</sup>C. Paz-Soldan, R. Nazikian, L. Cui, B. Lyons, D. Orlov, A. Kirk, N. Logan, T. Osborne, W. Suttrop, and D. Weisberg, “The effect of plasma shape and neutral beam mix on the rotation threshold for RMP-ELM suppression,” *Nucl. Fusion* **59**, 056012 (2019).
  - <sup>32</sup>B. Wan, Y. Liang, X. Gong, N. Xiang, G. Xu, Y. Sun, L. Wang, J. Qian, H. Liu, L. Zeng, L. Zhang, X. Zhang, B. Ding, Q. Zang, B. Lyu, A. Garofalo, A. Ekedahl, M. Li, F. Ding, S. Ding, H. Du, D. Kong, Y. Yu, Y. Yang, Z. Luo, J. Huang, T. Zhang, Y. Zhang, G. Li, and T. Xia, “Recent advances in EAST physics experiments in support of steady-state operation for ITER and CFETR,” *Nucl. Fusion* **59**, 112003 (2019).
  - <sup>33</sup>Y. Sun, M. Jia, Q. Zang, L. Wang, Y. Liang, Y. Liu, X. Yang, W. Guo, S. Gu, Y. Li, B. Lyu, H. Zhao, Y. Liu, T. Zhang, G. Li, J. Qian, L. Xu, N. Chu, H. Wang, T. Shi, K. He, D. Chen, B. Shen, X. Gong, X. Ji, S. Wang, M. Qi, Q. Yuan, Z. Sheng, G. Gao, Y. Song, P. Fu, B. Wan, and EAST Contributors, “Edge localized mode control using  $n=1$  resonant magnetic perturbation in the EAST tokamak,” *Nucl. Fusion* **57**, 036007 (2017).
  - <sup>34</sup>D. M. Yao, G. N. Luo, Z. B. Zhou, L. Cao, Q. Li, W. J. Wang, L. Li, S. G. Qin, Y. L. Shi, G. H. Liu, and J. G. Li, “Design, R&D and commissioning of EAST tungsten divertor,” *Phys. Scr.* **T167**, 014003 (2015).
  - <sup>35</sup>S. Wang, X. Ji, Y. Song, S. Zhang, Z. Wang, Y. Sun, M. Qi, X. Liu, S. Wang, and D. Yao, “Thermo-mechanical analysis of RMP coil system for EAST tokamak,” in *Proceedings of the 11th International Symposium on Fusion Nuclear Technology-11 (ISFNT-11) Barcelona, Spain, 15–20 September, 2013*, [Fusion Eng. Des. **89**, 991–995 (2014)].
  - <sup>36</sup>M. Jia, Y. Sun, F. Zhong, H. Li, G. Li, L. Wang, K. Gan, B. Zhang, J. Qian, and B. Shen, “Vacuum modeling of three-dimensional magnetic field topology under resonant magnetic perturbations on EAST,” *Plasma Phys. Controlled Fusion* **58**, 055010 (2016).
  - <sup>37</sup>X. Yang, Y. Sun, Y. Liu, S. Gu, Y. Liu, H. Wang, L. Zhou, and W. Guo, “Modelling of plasma response to 3D external magnetic field perturbations in EAST,” *Plasma Phys. Controlled Fusion* **58**, 114006 (2016).
  - <sup>38</sup>Y. Liu, A. Kirk, and E. Nardon, “Full toroidal plasma response to externally applied nonaxisymmetric magnetic fields,” *Phys. Plasmas* **17**, 122502 (2010).
  - <sup>39</sup>A. Bondeson, G. Vlad, and H. Lütjens, “Resistive toroidal stability of internal kink modes in circular and shaped tokamaks,” *Phys. Fluids B* **4**, 1889–1900 (1992).
  - <sup>40</sup>A. Wingen, T. E. Evans, and K. H. Spatschek, “Footprint structures due to resonant magnetic perturbations in DIII-D,” *Phys. Plasmas* **16**, 042504 (2009).
  - <sup>41</sup>Z. Xu, Z. W. Wu, W. Gao, Y. J. Chen, C. R. Wu, L. Zhang, J. Huang, J. F. Chang, X. J. Yao, W. Gao, P. F. Zhang, Z. Jin, Y. M. Hou, and H. Y. Guo, “Filterscope diagnostic system on the experimental advanced superconducting tokamak (EAST),” *Rev. Sci. Instrum.* **87**, 11D429 (2016).
  - <sup>42</sup>J. C. Xu, L. Wang, G. S. Xu, G. N. Luo, D. M. Yao, Q. Li, L. Cao, L. Chen, W. Zhang, S. C. Liu, H. Q. Wang, M. N. Jia, W. Feng, G. Z. Deng, L. Q. Hu, B. N. Wan, J. Li, Y. W. Sun, and H. Y. Guo, “Upgrade of Langmuir probe diagnostic in ITER-like tungsten mono-block divertor on experimental advanced superconducting tokamak,” *Rev. Sci. Instrum.* **87**, 083504 (2016).
  - <sup>43</sup>L. Wang, G. Xu, H. Guo, R. Chen, S. Ding, K. Gan, X. Gao, X. Gong, M. Jiang, P. Liu, S. Liu, G. Luo, T. Ming, B. Wan, D. Wang, F. Wang, H. Wang, Z. Wu, N. Yan, L. Zhang, W. Zhang, X. Zhang, S. Zhu, and the EAST Team, “Particle and power deposition on divertor targets in east h-mode plasmas,” *Nucl. Fusion* **52**, 063024 (2012).
  - <sup>44</sup>Z. Yang, Y. Wang, C. Zhang, P. He, S. Shu, J. Zhang, and B. Tang, “Techniques used for registration and reconditioning of infrared images of the experimental advanced superconducting tokamak (EAST) divertor,” *J. Fusion Energy* **39**, 184–191 (2020).
  - <sup>45</sup>J. Y. Zhang, B. Zhang, X. Gong, J. Chang, M. N. Jia, C. Liu, R. R. Liang, W. L. Chen, C. H. Wu, and S. Feng, “Development of a new dynamic foveated imager on wide-angle infra-red thermography system to improve local spatial resolution in EAST,” *Rev. Sci. Instrum.* **91**, 116101 (2020).
  - <sup>46</sup>H. Mao, F. Ding, G.-N. Luo, Z. Hu, X. Chen, F. Xu, Z. Yang, J. Chen, L. Wang, R. Ding, L. Zhang, W. Gao, J. Xu, and C. Wu, “A multichannel visible spectroscopy system for the ITER-like W divertor on east,” *Rev. Sci. Instrum.* **88**, 043502 (2017).
  - <sup>47</sup>J. Ren, Y.-W. Sun, H.-H. Wang, S. Gu, J.-P. Qian, T.-H. Shi, B. Shen, Y.-Q. Liu, W.-F. Guo, N. Chu, K.-Y. He, M.-N. Jia, Y. Wang, Z.-C. Sheng, Z.-P. Luo, L. Zeng, X.-Z. Gong, Y.-F. Liang, and B.-N. Wan, “Penetration of  $n=2$  resonant magnetic field perturbations in EAST,” *Nucl. Fusion* **61**, 056007 (2021).
  - <sup>48</sup>L. Zhang, S. Morita, Z. Xu, Z. Wu, P. Zhang, C. Wu, W. Gao, T. Ohishi, M. Goto, J. Shen, Y. Chen, X. Liu, Y. Wang, C. Dong, H. Zhang, X. Huang, X. Gong, L. Hu, J. Chen, X. Zhang, B. Wan, and J. Li, “A fast-time-response extreme ultraviolet spectrometer for measurement of impurity line emissions in the experimental advanced superconducting tokamak,” *Rev. Sci. Instrum.* **86**, 123509 (2015).
  - <sup>49</sup>Z. Xu, L. Zhang, Y. Cheng, S. Morita, L. Li, W. Zhang, F. Zhang, Z. Zhao, T. Zhou, Z. Wu, X. Lin, X. Gao, X. Ding, Y. Yang, and H. Liu, “An extreme ultraviolet spectrometer working at 10–130 Å for tungsten spectra observation with high spectral resolution and fast-time response in experimental advanced superconducting tokamak,” *Nucl. Instrum. Methods Phys. Res., Sect. A* **1010**, 165545 (2021).
  - <sup>50</sup>R. Nazikian, C. Paz-Soldan, J. D. Callen, J. S. deGrassie, D. Eldon, T. E. Evans, N. M. Ferraro, B. A. Grierson, R. J. Groebner, S. R. Haskey, C. C. Hegna, J. D. King, N. C. Logan, G. R. McKee, R. A. Moyer, M. Okabayashi, D. M. Orlov, T. H. Osborne, J.-K. Park, T. L. Rhodes, M. W. Shafer, P. B. Snyder, W. M. Solomon, E. J. Strait, and M. R. Wade, “Pedestal bifurcation and resonant field penetration at the threshold of edge-localized mode suppression in the DIII-D tokamak,” *Phys. Rev. Lett.* **114**, 105002 (2015).
  - <sup>51</sup>S. Gu, C. Paz-Soldan, Y. Q. Liu, Y. Sun, B. C. Lyons, D. A. Ryan, D. Weisberg, N. Leuthold, M. Willensdorfer, W. Suttrop, J.-K. Park, N. C. Logan, M. W. Shafer, H. H. Wang, Q. Ma, A. Kirk, B. Tal, M. Griener, ASDEX Upgrade, and EUROfusion MST1 Teams, “Influence of triangularity on the plasma response to resonant magnetic perturbations,” *Nucl. Fusion* **62**, 076031 (2022).
  - <sup>52</sup>Y. Liang, P. Lomas, I. Nunes, M. Gryaznevich, M. Beurskens, S. Brezinsek, J. Coenen, P. Denner, T. Eich, L. Frassinetti, S. Gerasimov, D. Harting, S. Jachmich, A. Meigs, J. Pearson, M. Rack, S. Saarelma, B. Sieglin, Y. Yang, L. Zeng, and JET-EFDA Contributors, “Mitigation of type-I ELMs with  $n=2$  fields on JET with ITER-like wall,” *Nucl. Fusion* **53**, 073036 (2013).
  - <sup>53</sup>N. Wang, Y. Liang, V. Igoshine, W. Suttrop, L. Li, M. Maraschek, M. Bernert, P. Denner, M. Faitsch, S. Fietz, Y. Gao, L. Giannone, A. Kirk, H. Meyer, F. Mink, P. Piovesan, The ASDEX Upgrade Team, and The EUROfusion MST1 Team, “Impact of  $n=1$  field on non-axisymmetric magnetic perturbations associated with the edge localized mode crashes in the ASDEX upgrade tokamak,” *Nucl. Fusion* **59**, 054002 (2019).